Tribology Letters (2026) 74:89
https://doi.org/10.1007/s11249-026-02186-1

ORIGINAL PAPER

Tribological Performance of MoS_2-Coated 6082-T6 Aluminium: Influence of Laser Texture Density and Pin-on-Disc Test Configuration

Juan Ignacio Ahuir-Torres[1] · Tahsin Tecelli Öpöz[1] · Guangyu Zhu[2] · Musa B. Bashir[3] · Hiren R. Kotadia[1]

Received: 15 April 2026 / Accepted: 23 July 2026 / Published online: 29 July 2026

Abstract
The 6082-T6 aluminium alloy is widely used in engineering applications but its broader deployment is restricted by poor wear and friction resistance. Solid lubricants such as molybdenum disulphide (MoS_2) can improve its tribological performance; however, their effectiveness is limited by short service life and the need for frequent replenishment. Laser surface texturing (LST) has proven effective in extending lubricant lifespan, yet the influence of tribological system configuration on textured, solid-lubricated aluminium surfaces remains insufficiently understood. In this study, the combined effects of groove texture density (TD) and pin-on-disc configuration on the tribological behaviour of MoS_2-coated 6082-T6 aluminium alloy were systematically investigated. Groove patterns with TD values ranging from 25 to 100% were fabricated using an infrared nanosecond pulsed fibre laser, and MoS_2 coatings were applied by spraying. Tribological performance was evaluated under dry and lubricated conditions using three configurations: textured pin, textured disc, and both pin and disc textured. Finite element analysis was conducted to examine the influence of surface texturing and groove orientation on compression and ejection normal stresses. Laser surface texturing extended the MoS_2 lubricant service life by approximately 2 to 50 times compared with non-textured surfaces, depending on TD and configuration. Increasing TD consistently enhanced lubricant lifespan. Among all configurations, the pin-and-disc system exhibited the longest service life, while the textured pin configuration showed the shortest. Finite element results identified ejection stress as the dominant factor governing lubricant depletion, providing new insight into stress-mediated solid lubrication mechanisms for 6082-T6 aluminium alloy.

Keywords Laser surface texturing · Pin-on-disc · Molybdenum disulphide · Aluminium alloy · Finite element analysis

1 Introduction

6082-T6 aluminum alloy (6082-T6) is widely used in aerospace, automotive, and energy applications due to its high strength-to-weight ratio, excellent corrosion resistance, and good formability [1–3]. Despite these advantages, its comparatively low hardness and strong adhesive tendencies lead to poor tribological behavior, particularly manifesting as high friction and accelerated wear. Consequently, the use of lubricants is often indispensable in applications involving 6082-T6 [4].

To overcome these limitations, a wide range of lubricants including solid (powders), semi-solid (greases), and liquid (oils and water-based solutions) has been explored. Solid lubricants are especially suitable for severe operating environments characterized by elevated temperatures, high loads, or vacuum conditions [5, 6]. Among them, molybdenum disulphide (MoS_2) is notable for its chemical inertness, low solubility, high wear resistance, and exceptionally low coefficient of friction [5, 7–9]. However, the durability of MoS_2 lubrication is constrained by gradual depletion during sliding, necessitating periodic replenishment to maintain performance.

Surface texturing has emerged as an effective strategy to mitigate lubricant depletion and extend lubrication lifespan. Engineered textures act as micro-reservoirs capable of storing and gradually releasing solid lubricant during sliding, compensating for material loss and prolonging the

✉ Juan Ignacio Ahuir-Torres
j.i.ahuirtorres@ljmu.ac.uk

1 School of Engineering and Built Environment, Liverpool John Moores University, Byrom Street, Liverpool L3 3AF, UK

2 School of Electrical Engineering, Chongqing University of Arts and Sciences, Chongqing 402159, China

3 Civil and Environmental Engineering, University of Liverpool, Liverpool L69 7ZX, UK

effectiveness of the coating. Additionally, textured features can entrap wear debris and thereby reduce abrasive interactions, further improving wear resistance [9–13]. A variety of methods have been employed to produce such textures, including mechanical machining [14], chemical etching [15], electrical discharge machining [16], plasma treatment [17], and laser processing [12, 18–20]. Of these, laser surface texturing (LST) is particularly attractive due to its environmental cleanliness, absence of tool wear, high reproducibility, capability for automation, and capacity for fabricating precise and diverse microgeometries [9, 12, 18, 19]. The availability of multiple laser types with differing wavelengths and pulse durations further enhances the flexibility of LST for tailoring surface architectures.

When applying LST to aluminum alloys such as 6082-T6, the choice of laser wavelength and pulse duration plays a critical role in determining texture quality. Ultraviolet lasers provide strong optical absorption in aluminum but are limited by operational complexity, high power consumption, and low pulse energy [21, 22]. Green lasers offer higher pulse energy and operational simplicity, although their absorption remains lower than that of ultraviolet sources [23, 24]. Infrared lasers, despite lower absorption, are widely used due to their significantly higher pulse energies and ease of operation [22]. Regarding pulse duration, nanosecond-pulsed lasers remain the most commonly adopted for LST because they limit the heat-affected zone (HAZ) while delivering sufficient energy for efficient ablation [25]. In contrast, continuous-wave, millisecond, and microsecond pulses generate excessive melt and a large HAZ, compromising texture precision [23]. Ultrashort pulsed sources (picosecond and femtosecond) minimize thermal effects but require substantially more pulses due to lower pulse energies, resulting in longer processing times [13, 18, 25, 26].

In addition to laser parameters, texture density (TD) is a critical factor governing the tribological response of textured, solid-lubricant-coated surfaces. TD influences both friction behaviour and lubricant lifespan [7–9, 12, 19, 20, 27–30]. However, the optimal TD is not universal; it depends on several interacting variables, including the solid lubricant type, texture geometry, substrate properties, lubricant deposition method, and importantly the nature of the tribological contact. While increasing TD may enhance performance under certain conditions, improvements are often confined to a specific TD range determined by the system's mechanical and kinematic characteristics [10, 20, 27]. To optimise texture design and better understand the mechanisms governing friction, wear, lubricant retention, and stress distribution, researchers have increasingly employed finite element analysis (FEA) as a complementary tool alongside experimental investigations. FEA enables detailed assessment of local contact conditions and provides valuable insight into the influence of texture geometry and density on tribological performance.

Finite element analysis has demonstrated to be a valuable tool for investigating the influence of laser-induced textures on the tribological properties of various systems. Uddin et al. [31] investigated the effect of the texture geometry, encompassing surface and 3D profile, as well as aspect ratio and texture density, on the tribological performance of the liquid-lubricated system under multidirectional sliding. Texture density was found to exert a higher influence on the friction coefficient than aspect ratio. Chevron, ellipsoid, and triangle geometry presented anisotropic tribological properties with respect to the sliding orientation. Zhang et al. [32] carried out a comparable investigation under single direction sliding conditions, employing different texture morphologies. Among the textures investigated, fish and bullet texture patterns exhibited the optimal stress distribution for the tribological properties. Lu et al. [33] utilized the same simulation methodology to determine the optimal texture pattern to improve the wear resistance of the cobalt alloy under sliding reciprocating conditions. Texture patterns investigated comprised dimples, groove, and grid configuration, with grid patterns yielding the lowest wear ratio, attributed to the uniform normal stresses distribution. Ahuir-Torres et al. [34] investigated the effect of the laser-induced texture pattern morphology on the lifespan of the MoS_2 lubricant under a ball-on-disc configuration employing finite element analysis. Groove pattern exhibited longer lubricant lifespan relative to the grid patterns, attributed to its more favorable normal stress distribution for the lubricant ejection. Collectively, these studies demonstrate that texture geometry and density significantly influence contact stress distribution, lubricant retention, friction behavior, and wear resistance. However, the optimal texture configuration remains highly dependent on the tribological system, lubrication mechanism, and operating conditions, highlighting the need for further investigation of texture design in solid-lubricated systems.

Although extensive studies have examined LST and MoS_2 lubrication on various metallic substrates [7–9, 12, 19, 20, 27–30], comparatively little work has focused on aluminium alloys such as 6082-T6. Moreover, the influence of tribological system configuration, whether the texture is applied to the pin, the disc, or both on the friction behaviour of solid-lubricated textured surfaces remains insufficiently understood. Most investigations focus on the surface texturing of a single contact body. These gaps limit the ability to design optimised surface architectures for MoS_2-assisted tribological systems involving aluminium alloys.

To address these shortcomings, the present study investigates the combined effects of groove-type texture density and tribological system configuration on the friction and wear behaviour of MoS_2-coated 6082-T6. Grooves were fabricated using an infrared nanosecond fibre laser under

Table 1 Chemical composition of 6082-T6 (wt%)

Element	Al	Si	Mg	Mn	Fe	Cu	Zn	Ti
Concentration (wt%)	96.82	1.00	0.90	0.70	0.25	0.05	0.10	0.05

scanning mode, with TD varied from 0 to 100%. Pin-on-disc tests were conducted under three configurations: (i) textured pin against smooth disc, (ii) textured disc against smooth pin, and (iii) both components textured. Finite element simulations were performed to evaluate how system conditions—including textured vs. non-textured surfaces, groove orientation relative to sliding direction, and contact body type—affect the spatial distribution of normal stress within the tribological interface. The resulting insights establish the optimal combination of texture density and system configuration required to maximise the tribological performance of MoS_2-coated 6082-T6.

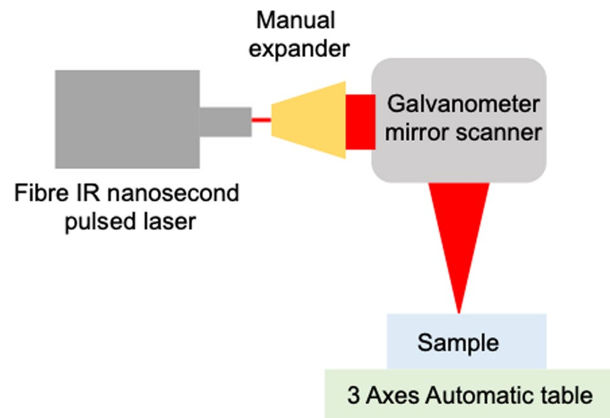

Fig. 1 Schematic of the laser surface texturing setup [34]

2 Experimental Set-Up and Methodology

2.1 Material

The tribological experiments employed 6082-T6 as the primary test material. Its chemical composition is presented in Table 1. Two sample geometries were prepared: (1) Discs (40 mm diameter, 3 mm thickness) used as the rotating component in the pin-on-disc tests, and (2) Cylindrical rods (6 mm diameter, 30 mm length) used as the stationary pins.

2.2 Laser Surface Texture

Prior to LST, samples were mechanically polished to a surface roughness (S_a) of approximately 100 nm using P1200 SiC abrasive paper, a condition recommended for optimal laser processing [35]. Samples were then cleaned following a multi-stage procedure consisting of detergent washing, a freshwater rinse, distilled water rinse, isopropanol spray, and heat drying. Groove patterns were selected as the texture geometry due to their extensive use and proven effectiveness in LST applications [36].

LST was performed using an infrared nanosecond-pulsed fiber laser (SPI Laser G3 20 W) equipped with a 1064 nm beam expander (Linos 2–8 ×), a galvanometric scanner (Nutfield Extreme-15-YAG) operated via SAM-Light v3.05 (SCAPS GmbH), and a 100 mm focal-length f-theta lens (Linos Ronar). Samples were mounted on a three-axis automated positioning stage (Aerotech Ltd., UK). A schematic of the system is shown in Fig. 1. The laser operated at 1064 ± 5 nm in TEM_{00} mode ($M^2 = 2.1$), with pulse durations between 9 and 200 ns and repetition frequencies of 1–500 kHz. The maximum average power and pulse energy before the optical system were 22 W and 880 μJ, respectively. The beam expander produced a 5.7 mm raw beam diameter. Beam steering via the galvanometer enabled scan speeds from 10^{-2} mm/s to 2×10^4 mm/s. Grooves were generated using a 400 μm defocused beam with overlapping pulses along the scanning direction.

TD of 25, 50, 75, and 100% were produced. Post-texturing, samples were cleaned using the same procedure described earlier. The complete set of LST parameters is provided in Table 2.

Table 2 Laser processing parameters used for surface texturing

Parameter	Value
Wavelength (nm)	1064 ± 5
Pulse length (ns)	200
Transverse electromagnetic mode	00
Focussing lens focal length (mm)	100.00
Raw beam diameter (mm)	5.7
Beam quality factor	2.1
Focused beam size (μm)	51
Rayleigh length (μm)	898
Distance to the focal point (μm)	400
Defocused beam size (μm)	56
Scan rate (mm/s)	625
Pulse repetition frequency (kHz)	25
Atmosphere	Air
Pulse energy (μJ)	236
Average power (W)	5.8

2.3 Tribological Tests

Tribological tests were carried out using a pin-on-disc apparatus (Koehler K93590) under three configurations (Fig. 2): (1) pin configuration: textured or non-textured 6082-T6 pin against an SAE 52100 steel disc. (2) disc configuration: SAE 52100 steel pin against a textured or non-textured 6082-T6 disc. (3) pin-and-disc configuration: textured or non-textured 6082-T6 pin against a textured or non-textured 6082-T6 disc. SAE 52100 steel counter bodies (6 mm × 30 mm pin; 100 mm × 30 mm disc) were supplied by Koehler Instruments. The tribological testing parameters were selected in accordance with ASTM G99-18 [37].

Tests were conducted under dry and MoS_2 conditions. Dry tests were performed only on non-textured 6082-T6 discs and used as a baseline. For lubricated tests, samples were coated with an aerosol spray with 70% in volume of MoS_2 purity and various organic binders (CRC "Dry Moly Lube", RS Components). Coatings were cured for 24 h, resulting in a final thickness of 15 ± 3 µm, measured by optical profilometry (Sect. 2.4). In the pin-and-disc configuration, both components were coated with MoS_2, while the SAE 52100 counter bodies remained uncoated throughout all tests.

Testing parameters are summarized in Table 3. Each test was repeated at least three times to ensure statistical significance. Error bars in all graphical results represent the standard deviation of the repeated measurements. It is important to note that the nominal contact pressure was calculated in accordance with ASTM G99-18 [37]. However, factors

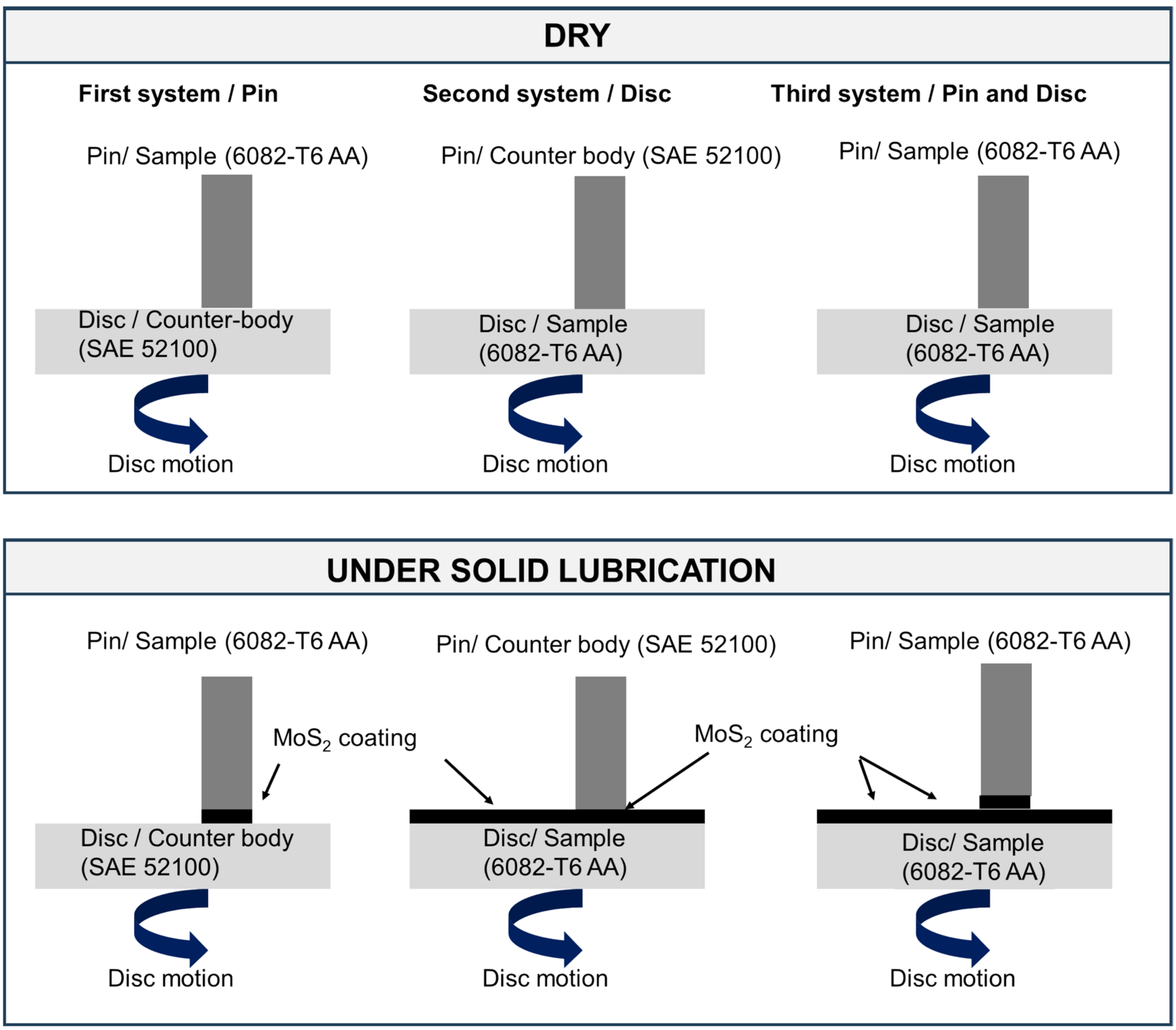

Fig. 2 Schematic representation of the three pin-on-disc test configurations used in this study with and without lubrication

Table 3 Pin-on-disc test parameters

Parameter	Value
Rotational speed (rpm)	100
Linear velocity (mm/s)	100
Worn track radius (mm)	10
Load (N)	10
Pressure (Pa)	354,000
Temperature (K)	298, room temperature
Humidity (%)	80, natural
Atmosphere	Natural air

such as surface roughness, plastic deformation, and texture geometry can locally alter the contact pressure distribution. To evaluate the influence of these factors on local contact stresses and pressure distribution, a series of finite element simulations were performed, as described in Sect. 3.

2.4 Characterization Methods

Surface topography and groove geometry were characterized using a Bruker ContourGT optical profiler operating in vertical scanning interferometry (VSI) mode with green light illumination and a 50 × objective. Groove width and depth were calculated by averaging measurements from ten randomly selected textured areas.

Surface morphology and chemical composition were analysed using a Hitachi TM4000 Plus SEM. Imaging was performed using secondary electron (SE) and backscattered electron (BSE) detectors at accelerating voltages of 5 and 15 kV, beam currents of 70 μA, and spot sizes of 2 and 3 μm. Elemental composition was obtained via energy-dispersive X-ray spectroscopy (EDS) using BSE detection at 15 kV and a spot size of 3 μm.

3 Finite Element Analysis Modeling

Finite element simulations were conducted to evaluate the influence of test configuration on normal stress distribution, a key parameter affecting solid-lubricant ejection and, consequently, lubricant lifespan [38]. All simulations were performed using ANSYS 2024.

Models were constructed for non-textured surfaces and textured surfaces with 75% TD on the pin, disc, and both components (Fig. 3). Geometries were scaled down to reduce computational cost: (1) Pin: 0.60 mm diameter, 1.50 mm length and (2) Disc: 1.50 × 1.50 × 1.5 mm.

Textured components were modeled as 6082-T6 Al, while non-textured surfaces were modeled as AISI 52100 steel. The physical properties of the materials were obtained from ANSYS 2024 library. Groove geometry (width, depth,

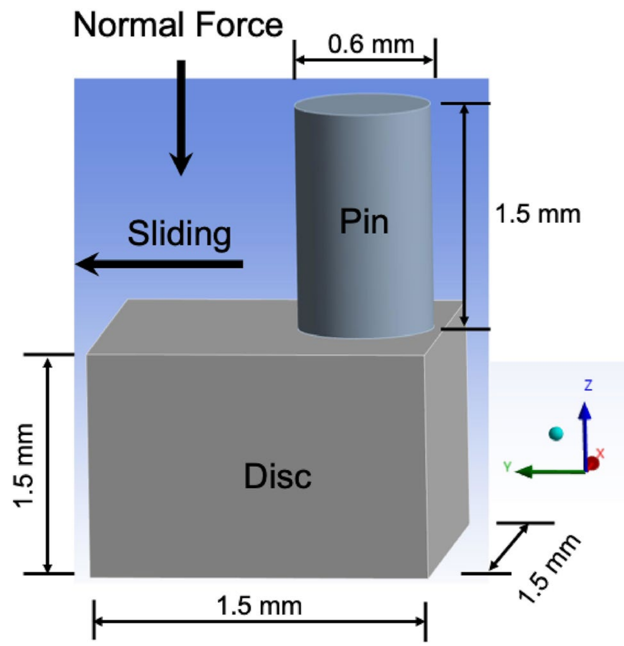

Fig. 3 Modeled system used for FEA simulation of the pin-on-disc configuration

and spacing) was taken from experimental measurements (Sect. 4.1). The disc center was positioned at the origin, and the pin center was placed at (X = 0, Y = −0.40 mm, Z = 1.55 mm). 2D shell elements with triangular meshes (0.01 mm element size) was used, approximately four times smaller than the groove width (~ 45 μm).

Contact between the bodies was dynamically updated during sliding. The coefficient of friction was set to 0.30 to represent the lubrication condition, consistent with lubricated experimental conditions (Sect. 4.2). A normal load of −0.10 N was applied to the pin to maintain the experimental contact pressure (354 kPa). Sliding motion was applied along the Y-axis at −0.10 ms^{-1}, with either the pin or disc displaced depending on the configuration. In the real situation, the linear velocity gradually varies as a function of the position into the pin for pin-on-disc configuration, ranging from 0.13 ms^{-1} at the position furthest from the rotational center to 0.07 ms^{-1} at the position closest to the rotational center. The linear velocity employed in the simulations thus corresponded to the average of two real linear velocity values. Notably, these simulations were conducted as a qualitative investigation of the tribological processes rather than a quantitative one. The non-moving body was fixed to prevent rigid-body motion. Gravity (9.807 N kg^{-1}) was included in all simulations.

Because the disc rotates during testing and the groove orientation is unidirectional, the relative alignment between grooves and sliding direction varies continuously. Therefore, simulations for textured surfaces were carried out under three scenarios (Fig. 4): (a) grooves perpendicular to sliding, (b) grooves at 45°, and (c) grooves parallel to sliding. These scenarios were unnecessary for non-textured surfaces, which are tribological isotropic.

Simulation assumptions: (1) Disc and pin dimensions were scaled down through the correct adjustment of the pressure. It is justified by the flat surfaces of the pin and the disc. In flat surfaces, the contact area is equivalent to the nominal surface area of the interacting bodies. (2) The applied normal force was directly adjusted to maintain the experimental contact pressure, which enabled by the relative flat surfaces of the bodies. (3) Groove-rim asperities were omitted because the MoS_2 coating fully covered the textured surface. (4) Material deformation was neglected, as MoS_2 lubrication mitigated the elastic–plastic deformation of the material under the tested conditions, which was also observed for similar conditions in C28000 brass [34]. (5) The temperature of the simulations was maintained constant, as the heat generated during the tribological testing is insufficient to melt the solid lubricant or alter its fluidity. (6) The coefficient of friction was assumed as 0.3 due to this value corresponding with the coefficient of friction measured during the effective lubrication service period, according to the experimental results (Sect. 4.2.3). (7) The lubrication capability of the solid lubricant was assumed to remain constant over time as these parameters were observed to be stable during the tribological testing until the failure of the lubricant for the experimental results (Sect. 4.2.3). Accordingly, these simulations were conducted to analyze the configuration and texture influence on the lubrication compression and ejection while the solid lubricant exhibited an effective lubrication effect.

4 Results

4.1 Surface Characterization

Optical profilometry confirmed that the laser-generated grooves consistently exhibited a spherical-cap cross-section (Fig. 5a and b), characteristic of U-type textures [39, 40]. This geometry arises because only the central portion of the Gaussian beam possesses sufficient energy fluence to induce material removal. Pronounced crests were observed along the groove edges. These are attributed to the hydrodynamic displacement of molten material and the recoil pressure acting on the melt during nanosecond-pulse ablation, followed by rapid solidification [36]. The average groove width and depth were 45 ± 4 and 4.5 ± 0.4 µm, respectively (Fig. 5b), giving a depth-to-width ratio of 0.1, a value commonly associated with favourable tribological behaviour under lubricated conditions [9, 41–43].

TD was determined from the groove width (w) and the spacing between adjacent grooves (l), Table 4, using Eq. (1) [34]. Notably, groove width encompassed both the crest and the valley regions; consequently, the groove patterns at 100% TD exhibited a slight degree of overlap between the crests of the adjacent grooves.

$$TD = 100 \times \frac{wl}{l^2} \qquad (1)$$

Laser texturing produced distinct modifications to the surface topography relative to the non-textured condition (Fig. 5). These morphological changes became more pronounced with increasing TD. At lower TD values, a relatively wide flat region remained between adjacent grooves; however, this region diminished progressively at higher TD. At 100% TD, the pattern differed notably: adjacent grooves were separated only by narrow walls (~ 10 µm wide) formed by consolidated crest material, giving the surface a more ridge-like texture. Sa increased with increasing TD, which is a well-established effect of the laser surface texturing.

SEM imaging (Fig. 6) revealed the presence of re-solidified ejected material surrounding all groove patterns, confirming that phase explosion was the dominant ablation mechanism. In nanosecond-laser ablation at high fluence, rapid superheating leads to the nucleation and expansion of liquid–vapour bubbles that rupture explosively, ejecting

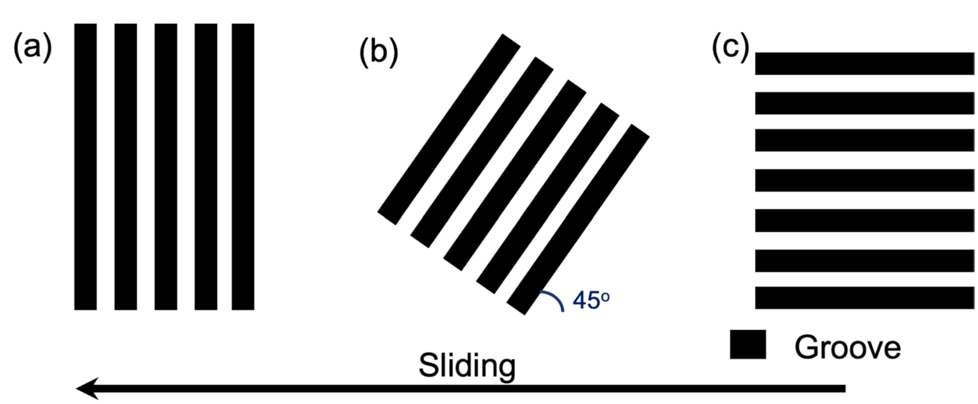

Fig. 4 Relative alignment between groove orientation and sliding direction: **a** perpendicular, **b** diagonal, **c** parallel

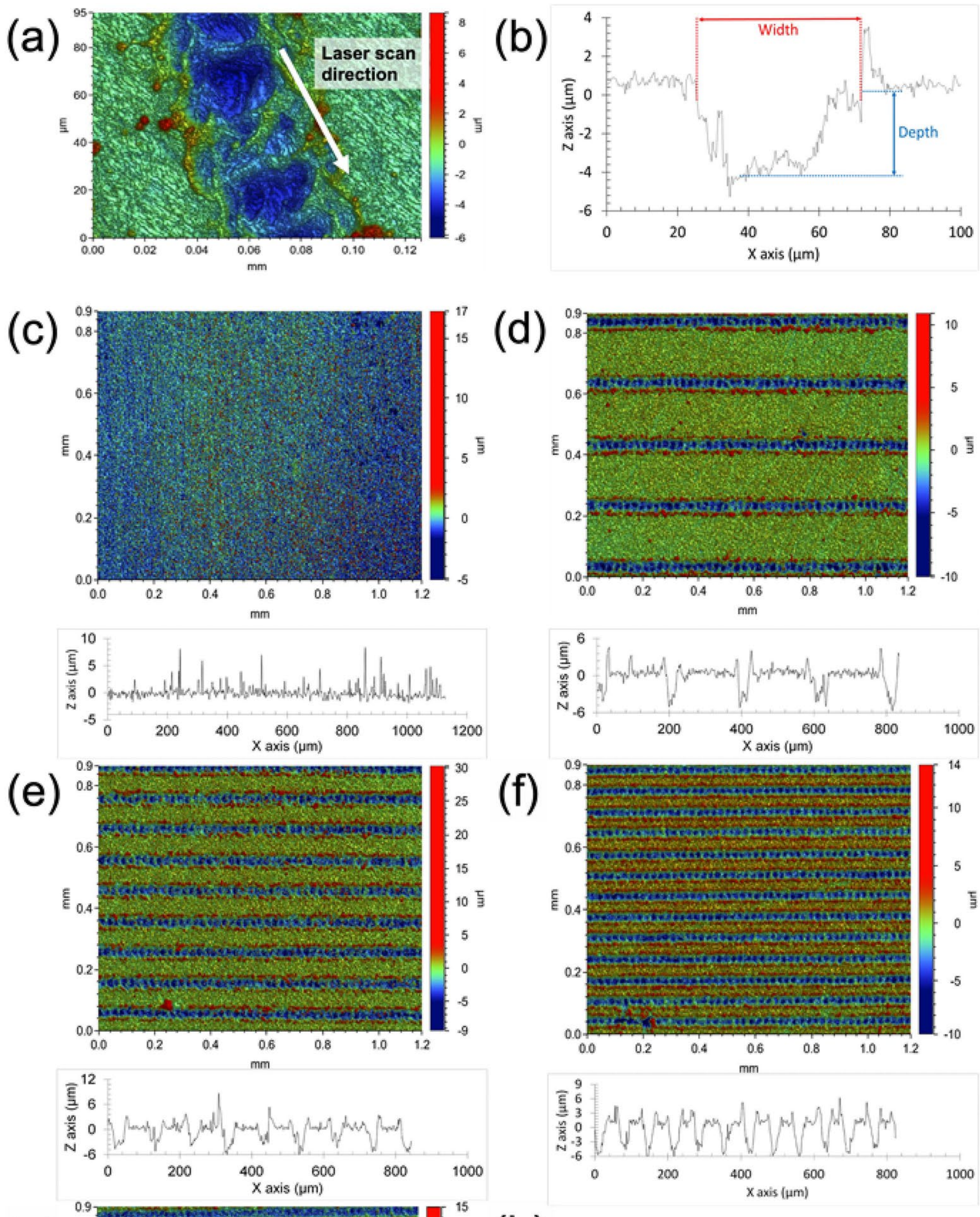

TD (%)	Sa (nm)
0	100 ± 10
25	1100 ± 100
50	1500 ± 100
75	1900 ± 100
100	2200 ± 100

Fig. 5 **a** and **b** Optical profilometry of a representative laser-induced groove: **a** 3D topography, **b** cross-sectional profile. Surface topography of **c** non-textured sample and **d**–**g** textured samples at TD values of **d** 25%, **e** 50%, **f** 75%, and **g** 100%. **h** Summary of average surface roughness (Sa)

Table 4 Lists the corresponding groove spacing used to produce TD values of 25–100%

TD(%)	25	50	75	100
l(μm)	180	90	60	45

molten material from the ablation site [44, 45]. The morphology of the redeposited material observed here is consistent with this mechanism.

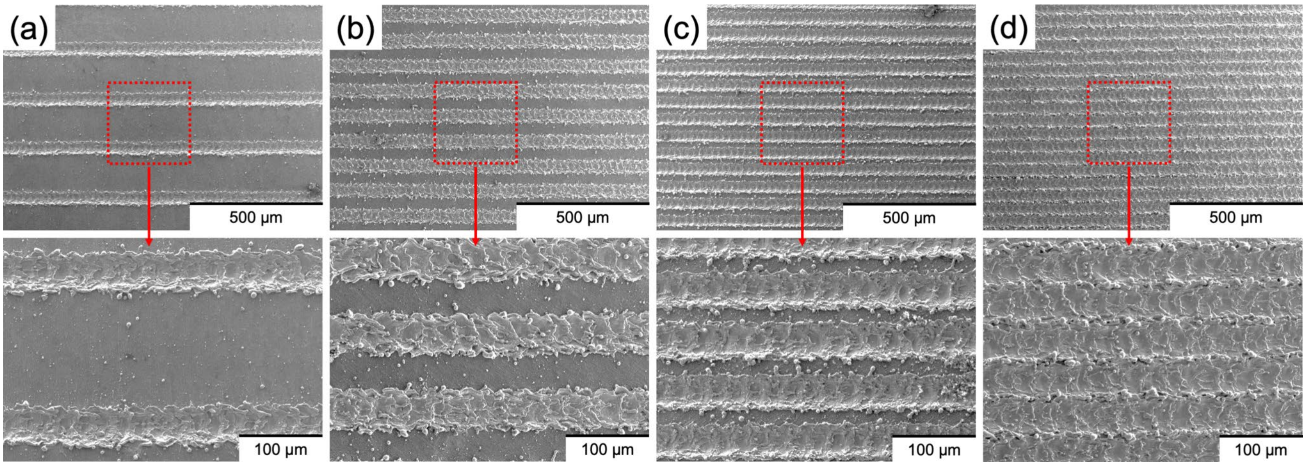

Fig. 6 SEM-SE images of groove patterns on 6082-T6 at TD values of **a** 25%, **b** 50%, **c** 75%, and **d** 100%

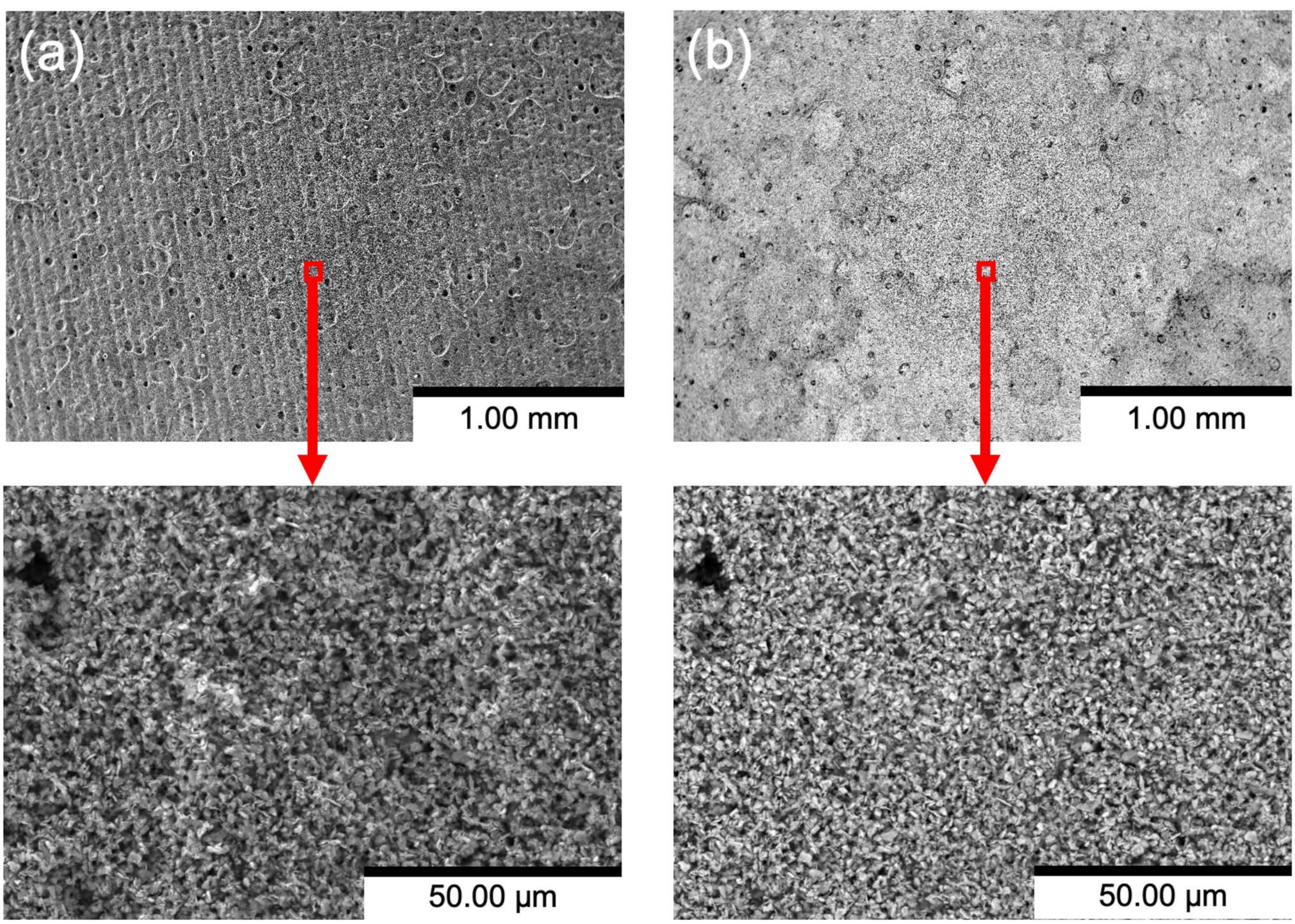

Fig. 7 SEM top-view images of MoS_2-coated groove patterns at 75% TD: **a** SE morphology, **b** BSE chemical contrast showing uniform coating distribution

Figure 7 shows the morphology and chemical distribution of the MoS_2-coated textured surfaces. The surface topography of the coated samples was significantly affected by the groove structure (Fig. 7a), confirming that the MoS_2 film (15 ± 3 μm) was sufficiently thin to be influenced by the laser-induced textures. BSE images (Fig. 7b) demonstrated uniform coating coverage across both groove interiors and crest regions. High-magnification SEM inspection indicated that the coating consisted of MoS_2 flakes with lateral dimensions of several hundred nanometres. Their nanoscale size enabled effective infiltration and anchoring within the textured grooves, ensuring adequate lubricant availability within the reservoirs.

4.2 Pin-on-Disc Testing Results (Lubricant Service Life)

4.2.1 Non-textured Samples in Dry and Under Lubrication Conditions (Reference Values)

Figure 8 presents the temporal evolution of the coefficient of friction for non-textured 6082-T6 samples tested under dry and MoS_2-lubricated conditions across the three pin-on-disc configurations. Under dry sliding, all configurations exhibited a rapid increase in coefficient of friction during the initial running-in stage, followed by a transition to a quasi-steady-state regime. The steady-state coefficient of friction stabilised at 0.75 ± 0.07, 0.90 ± 0.08, and 0.70 ± 0.07 for the pin, disc, and pin-and-disc configurations, respectively. These steady-state dry friction values were subsequently used as reference thresholds to define the loss of lubricating effectiveness of the MoS_2 coating. It is important to note that coefficient of friction

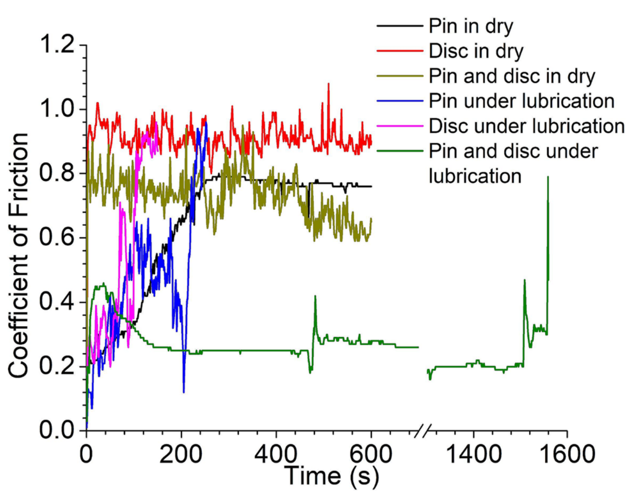

Fig. 8 Temporal evolution of the coefficient of friction for non-textured 6082-T6 samples under dry and MoS_2-lubricated conditions across the three pin-on-disc configurations

thresholds associated with the lubrication lifespan were exclusively defined by the configuration of the tribological testing, as the lubricant coating was completely removed. Specifically, the MoS_2 layer was considered functional if the measured coefficient of friction remained below the corresponding dry friction level for each configuration [9, 11, 46].

Under MoS_2 lubrication, all non-textured samples exhibited an initially reduced coefficient of friction, ranging between 0.2 and 0.5, depending on the test configuration. Although solid lubricants such as MoS_2 can theoretically achieve friction coefficients as low as 0.03, practical values are often higher due to variations in surface roughness, coating thickness, contact pressure, coating microstructure, and test conditions [1, 7, 9]. After a configuration-dependent sliding duration, the coefficient of friction increased abruptly to values comparable to those observed under dry conditions, indicating the depletion or failure of the MoS_2 lubricating layer [11, 46, 47]. The duration of this low-friction regime, defined here as the lubricant service life, varied markedly with the test configuration. The service life was measured as 210 s for the pin configuration, 95 s for the disc configuration, and 1550 s for the pin-and-disc configuration.

The longer service life observed in the pin configuration compared to the disc configuration can be attributed to differences in lubricant loss mechanisms. In the pin configuration, MoS_2 applied to the pin surface initially adheres to the steel disc under contact pressure. During sliding, the transferred MoS_2 accumulates preferentially along the edges of the wear track on the disc, effectively delaying loss of tribological effectiveness from the contact zone [48]. Conversely, in the disc configuration, lubricant loss occurs through a combination of adhesion to the pin surface and mechanical dragging of the MoS_2 film by the leading edge of the pin, resulting in more rapid depletion of the lubricant layer [18, 46, 49]. Although the disc configuration exhibits a larger rubbishing area, which may delay the loss lubricant efficiency through the mitigation of thermal abrasive particle formation, the increased probability of the localised lubricant failure with the enhancement in the rubbishing area neutralises this beneficial effect on the lubrication performance.

The pin-and-disc configuration exhibited the longest lubricant service life among all non-textured cases. This behaviour is primarily attributed to the presence of MoS_2 coatings on both contacting surfaces, effectively doubling the available lubricant thickness. Since lubricant service life is directly proportional to coating thickness [1, 7, 9], this configuration inherently sustains lubrication for a longer duration. Additionally, lubricant removal in this configuration is dominated by dragging mechanisms rather than adhesion-driven transfer, further contributing to the extended service life.

These lubricant service life values for non-textured samples provide essential baseline reference points against which the influence of laser-induced texture density on lubricated tribological performance is evaluated in subsequent sections.

4.2.2 Influence of TD on Lubricant Service Life

All laser-textured samples exhibited a substantial increase in lubricant service life compared with non-textured references across all test configurations (Fig. 9). This enhancement is primarily associated with the role of groove textures as solid lubricant reservoirs. During sliding, localised contact pressures combined with relative motion promote the gradual release of MoS_2 from the grooves into the contact interface. This continuous lubricant supply compensates for lubricant loss during testing, thereby stabilising the coating and extending its effective lifetime [4, 11, 28, 46]. The grooves further act as traps for wear debris generated during sliding. Debris accumulation within the contact interface can disrupt lubricant adhesion and accelerate coating failure; therefore, its sequestration within the textures further contributes to improved lubricant durability [11, 47, 49].

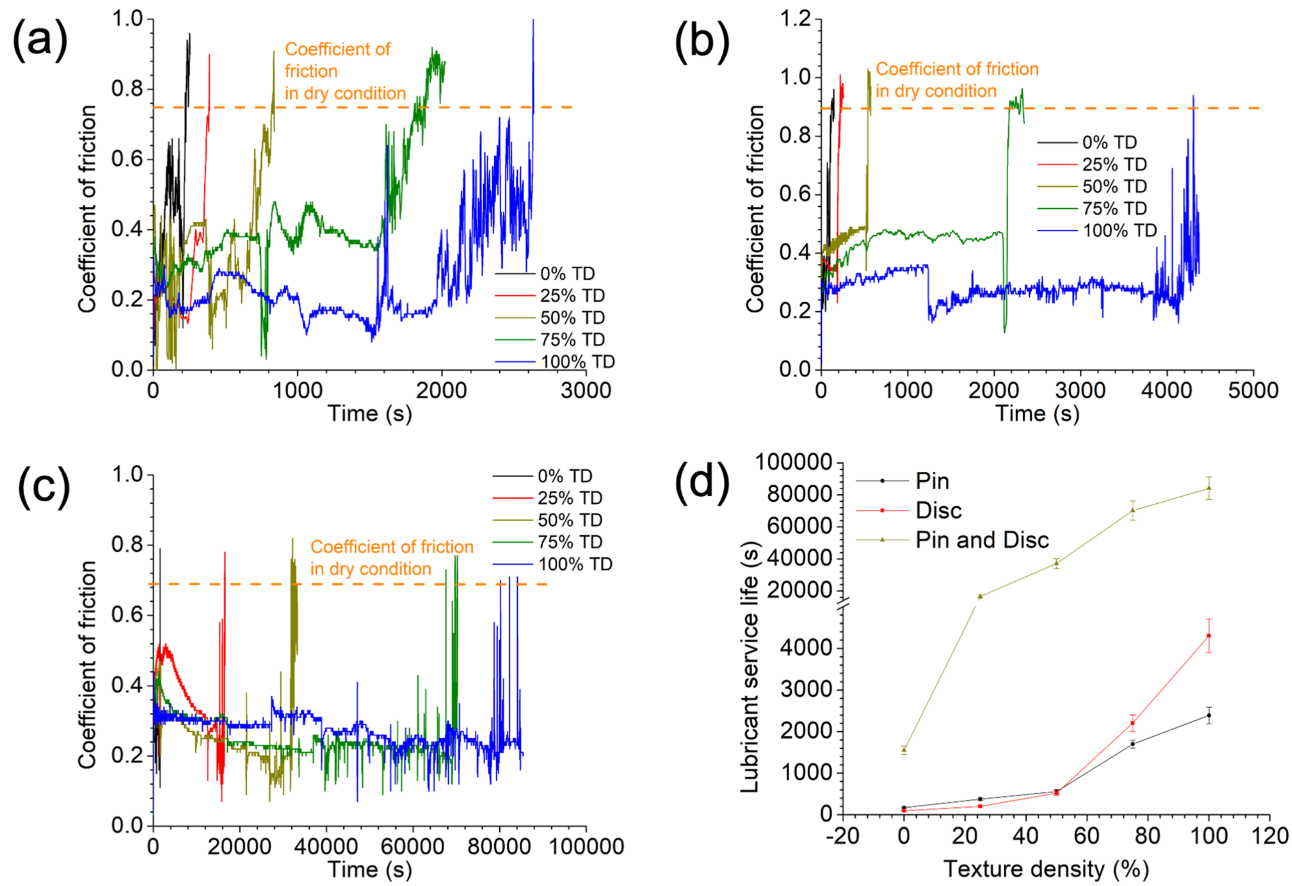

(e)

TD (%)	Configuration		
	Pin	Disc	Pin and Disc
0	170 ± 10	95 ± 90	1550 ± 90
25	380 ± 30	200 ± 20	16500 ± 900
50	560 ± 50	520 ± 40	37000 ± 2000
75	1700 ± 90	2200 ± 100	70000 ± 5000
100	2390 ± 90	4300 ± 400	84000 ± 6000

Fig. 9 Evolution of the coefficient of friction under MoS_2 lubrication for non-textured and textured 6082-T6 samples with TD values of 25, 50, 75, and 100% for **a** pin configuration, **b** disc configuration, and **c** pin-and-disc configuration. **d** Graph and **e** table of the lubricant service life as a function of texture density for all configurations

For all configurations, the lubricant service life increased systematically with increasing TD (Fig. 9d), reaching values up to approximately 50 times higher than those of non-textured samples under optimal conditions. This trend is attributed to the greater volume of MoS_2 retained within denser groove patterns, as the amount of stored lubricant scales directly with the surface coverage of the texture [19, 28, 47]. Higher TD also reduces the spacing between grooves, thereby limiting the extent of non-textured regions where the MoS_2 coating is thinner and more susceptible to premature failure. Since lubricant service life is strongly dependent on coating thickness, reducing these weak regions delays the onset of lubricant depletion [1, 7, 9]. Surfaces with higher TD moreover provide a greater number of cavities, enhancing debris entrapment efficiency and further stabilising the lubricant layer [11, 47, 49].

Among all configurations, the pin-and-disc configuration consistently delivered the longest lubricant service life at every TD level, exceeding the other configurations by a factor of approximately two to four. This superior performance results from the combined effects of a doubled MoS_2 coating thickness on both contacting surfaces [1, 7, 9], an increased total lubricant reservoir capacity due to texturing of both bodies [19, 28, 47], and improved debris trapping efficiency [11, 47, 49]. In addition, a lubricant feedback mechanism is enabled in this configuration: MoS_2 detached from one surface can be re-captured by the textured grooves on the opposing surface, contributing to partial coating restoration and sustained lubrication.

At lower TD values (25 and 50%), the lubricant service lives of the pin and disc configurations were comparable. However, at higher TD values (75 and 100%), the disc configuration exhibited a noticeably longer service life than the pin configuration. This behavior is attributed to differences in the spatial distribution and magnitude of normal stress acting on the textured surfaces. Normal stress governs the rate at which lubricant is ejected from surface reservoirs, thereby influencing lubricant depletion kinetics [48]. The contrasting stress distributions associated with pin and disc texturing become increasingly influential at higher TD, where texture–contact interactions are more pronounced. A detailed analysis of normal stress distribution and its effect on lubricant ejection is presented in Sect. 4.3.

The increase in Sa associated with the enhancement in TD exhibited negligible effect on the coefficient of friction of the samples, indicating the minimum influence of this factor in the friction under investigated conditions.

4.3 Finite Element Analysis Simulation

FEA revealed that the magnitude and spatial distribution of normal stress on both the pin and disc surfaces depend strongly on (i) the presence or absence of surface texturing, (ii) the body considered (pin or disc), and (iii) the relative orientation between the groove pattern and the sliding direction (Fig. 10). In the simulations, positive normal stress values indicate stress acting in the opposite direction to the applied load direction, whereas negative values correspond to stress acting in the direction of the applied load direction. Accordingly, positive normal stresses were classified as ejection stresses for the disc and compression stresses for the pin. Conversely, negative normal stresses were considered compression stresses for the disc and ejection stresses for the pin. Notably, the groove bottom of the disc was oriented in the applied load direction, while the groove bottom of the pin was localized in the opposite to the applied load direction. This distinction is critical, as ejection stresses govern the rate of solid-lubricated expulsion from the surface reservoirs, directly influencing lubricant service life.

4.3.1 Non-textured Surfaces

Non-textured surfaces exhibited exclusively ejection stresses on both contacting bodies (Fig. 10a), as the applied load from the opposing body induces stress acting opposite to the coated surface [50]. The spatial distribution of the normal stress closely followed the geometry of each body, appearing square-shaped for the disc and circular for the pin. This stress distribution observed on the disc is attributed to its limited dimensions, which preclude the full observation of the characteristic circular stress distribution. However, the maximum concentration of both negative and positive stresses remains localized within the contact area [50]. In both cases, the maximum absolute normal stress occurred at the center of the contact region. Notably, the disc surface exhibited a more gradual spatial variation of normal stress compared with the pin, which displayed a steeper stress gradient. These observations confirm that body geometry plays a dominant role in controlling normal stress distribution in non-textured contacts [50].

4.3.2 Effect of Surface Texturing

The introduction of groove textures significantly altered both the type and spatial distribution of normal stresses, producing coexisting regions of compression and ejection stresses on the same surface (Fig. 10b–e). For both pin and disc, compression stresses were typically located near geometric boundaries, while ejection stresses were concentrated within or near the groove features. The coexistence of these two stress types is beneficial for solid lubrication, as compression stresses favor lubricant retention within the grooves, whereas ejection stresses promote controlled lubricant release into the contact interface [34, 38].

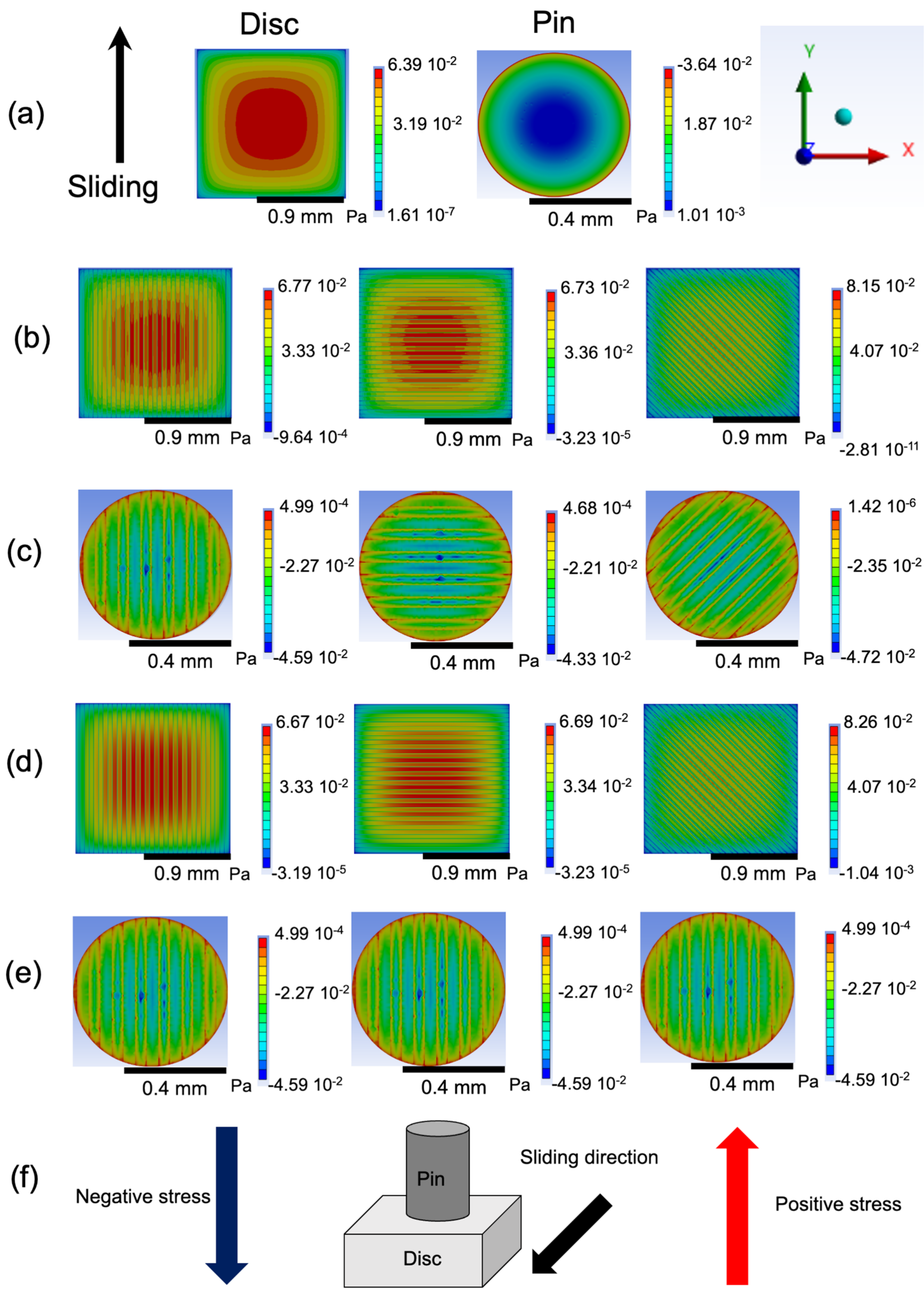
Disc
Pin
(a)
Sliding
0.9 mm
Pa
6.39 10-2
3.19 10-2
1.61 10-7
0.4 mm
Pa
-3.64 10-2
1.87 10-2
1.01 10-3
Y
X
Z
(b)
0.9 mm
Pa
6.77 10-2
3.33 10-2
-9.64 10-4
6.73 10-2
3.36 10-2
-3.23 10-5
8.15 10-2
4.07 10-2
-2.81 10-11
(c)
0.4 mm
Pa
4.99 10-4
-2.27 10-2
-4.59 10-2
4.68 10-4
-2.21 10-2
-4.33 10-2
1.42 10-6
-2.35 10-2
-4.72 10-2
(d)
6.67 10-2
3.33 10-2
-3.19 10-5
6.69 10-2
3.34 10-2
-3.23 10-5
8.26 10-2
4.07 10-2
-1.04 10-3
(e)
4.99 10-4
-2.27 10-2
-4.59 10-2
(f)
Negative stress
Pin
Disc
Sliding direction
Positive stress

◂**Fig. 10** Spatial distribution of normal stress on pin and disc surfaces for **a** non-textured and textured configurations: **b** textured disc, **c** textured pin, **d** textured disc in pin-and-disc configuration, and **e** textured pin in pin-and-disc configuration. **f** Schematic drawing of the negative and positive stress direction

4.3.2.1 Textured Disc For the textured disc, the relative orientation between the grooves and the sliding direction exerted a pronounced influence on normal stress distribution (Fig. 10b). When grooves were oriented parallel or perpendicular to the sliding direction, the highest ejection stresses were predominantly localised within the grooves, while the inter-groove regions experienced comparatively lower ejection stresses. This distribution supports sustained lubrication by enabling gradual lubricant release while preserving lubricant reservoirs [34, 38]. In both orientations, the regions of high ejection stress extended along the groove direction. In contrast, when the grooves were oriented at 45° to the sliding direction, the highest ejection stresses became localised at the bases of the central grooves, whereas the groove edges experienced lower ejection stresses. Such a highly heterogeneous stress distribution can adversely affect lubrication efficiency, as excessive stress localisation can disrupt the balance between lubricant expulsion and retention within the textured cavities [34].

4.3.2.2 Textured Pin For the textured pin, ejection stresses were also concentrated on the grooves; however, their spatial distribution was markedly more localized and heterogeneous than for the disc (Fig. 10c). Compression stresses appeared sporadically along groove edges, while ejection stresses were predominantly located within inter-groove regions. This stress pattern reduces the effectiveness of the groove structure in maintaining stable solid lubrication, as excessive heterogeneity weakens the balance between lubricant ejection and reservoir replenishment [34]. Importantly, this stress distribution was largely independent of groove orientation, indicating that pin geometry dominates stress evolution in this configuration.

4.3.2.3 Textured Pin-and-Disc Configuration When both pin and disc were textured, the normal stress distribution on the disc varied with groove orientation (Fig. 10d), while the stress distribution on the pin remained essentially insensitive to orientation (Fig. 10e). The stress profiles on the disc closely resembled those observed for the textured-disc-only configuration, albeit with a more homogeneous spatial distribution. This indicates that counterbody topography exerts a limited influence on the stress distribution of the textured surface in contact.

4.3.3 Maximum and Minimum Normal Stresses

Figure 11 summarises the maximum and minimum normal stress values extracted from all simulated configurations. These values varied significantly with body geometry, surface texturing, and groove orientation—factors known to strongly influence solid lubrication performance [34].

Minimum normal stresses were negative for most configurations, indicating compression, with the sole exception of the non-textured disc, which exhibited a positive minimum value. Conversely, maximum normal stresses were predominantly positive (ejection stresses), except for the non-textured pin, which showed a compressive maximum.

The non-textured disc exhibited a higher maximum ejection stress (in absolute terms) than the corresponding value for the pin. This elevated ejection stress explains the shorter lubricant service life observed experimentally for the disc configuration relative to the pin configuration in non-textured systems. Since the solid lubricant ejection rate is proportional to the magnitude of the normal stress acting away from the coated surface, higher ejection stresses accelerate MoS_2 depletion [34].

For textured surfaces, both ejection and compression stresses were present, and their magnitudes depended on the body type and groove orientation. Across all textured configurations, the disc consistently exhibited higher ejection stresses and lower compression stresses than the pin. This indicates that ejection stresses play a more dominant role in governing lubricant service life than compression stresses. The difference between ejection and compression stresses further was more pronounced for the disc than for the pin. Previous studies have shown that an increase in this stress differential can enhance lubrication efficiency, although excessively large differences may become detrimental [34].

For groove patterns on the disc, both compression and ejection stresses were strongly influenced by groove orientation. When only the disc was textured, the highest compression stress occurred for grooves parallel to the sliding direction, while the lowest was observed at 45°. In contrast, ejection stresses were comparable for parallel and perpendicular orientations, with the highest ejection stress occurring at 45°. When both pin and disc were textured, disc ejection stresses followed a similar trend, whereas compression stresses differed: the diagonal orientation (45°) produced the highest compression stress, while parallel and perpendicular orientations yielded similar values.

For groove patterns on the pin, both compression and ejection stresses were comparatively insensitive to configuration and groove orientation, exhibiting similar magnitudes across most cases. The only notable exception occurred for the textured-pin-only configuration with grooves oriented at 45°, where compression stress reached its lowest value. In all cases, ejection stresses exceeded compression stresses.

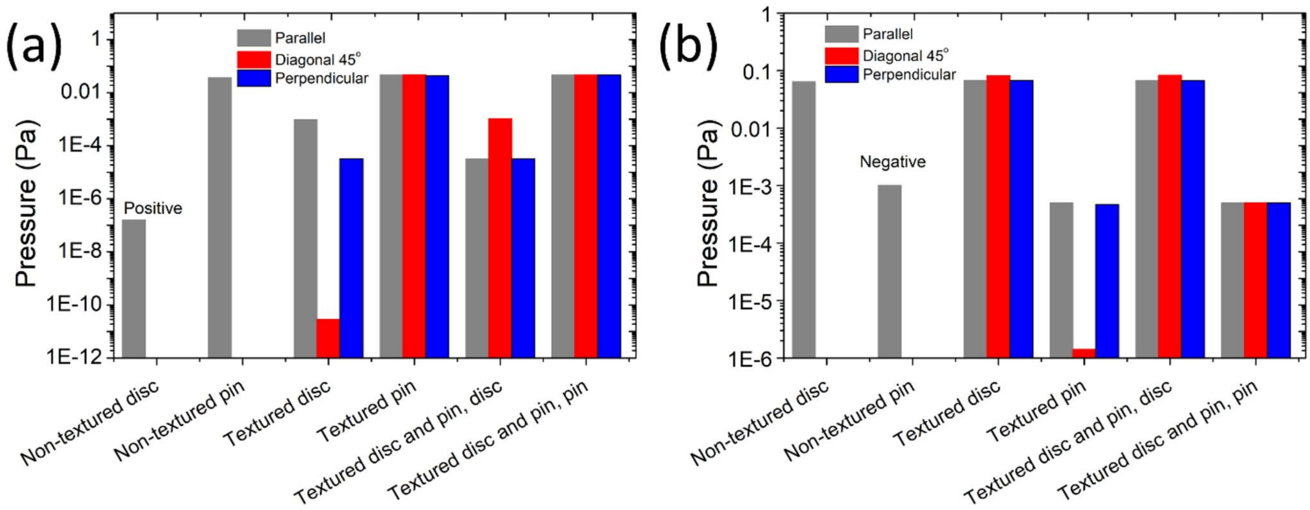

Fig. 11 **a** Minimum and **b** maximum normal stresses obtained from finite element simulations. Minimum stresses were positive only for the non-textured disc, while maximum stresses were compressive only for the non-textured pin

4.4 Worn Groove Assessment

Post-tribological examination of the laser-textured samples revealed localised wear within the groove patterns (Fig. 12), indicating regions where the MoS_2 coating had failed. The MoS_2 layer exhibited non-uniform thickness across the 6082-T6 surface, and thinner regions were more susceptible to accelerated wear. Once the coating was locally depleted, direct metal-to-metal contact occurred, leading to the initiation of abrasive wear mechanisms [4, 28]. Despite differences in texture density and test configuration, all samples displayed similar wear-track morphologies after complete lubricant failure.

SEM observations of the worn grooves showed the presence of transferred layers, scratches, and particulate debris. Detached material from the sample surface was observed to re-adhere locally, likely through friction-induced adhesion or micro-scale friction welding processes [4, 12, 47]. The scratches observed within the grooves were primarily attributed to abrasive wear caused by hard debris particles generated during sliding. Frictional heating during testing converted part of the kinetic energy into thermal energy, locally increasing the surface temperature. This thermal activation facilitated oxidation of detached aluminium debris in the presence of atmospheric oxygen. The resulting hard oxide particles subsequently acted as third-body abrasives, producing additional scratching within the wear tracks [19, 47]. The observed particles comprised a mixture of wear debris and adhered MoS_2 flakes, which were likely transferred from the counter-body surface and redeposited within the grooves [4, 47].

EDS elemental mapping of the worn grooves revealed a heterogeneous distribution of Al, S, Mo, and O (Fig. 13). Elevated aluminium concentrations were detected within the worn groove regions, accompanied by markedly reduced sulphur and molybdenum signals, indicating substantial removal of the MoS_2 coating. Nevertheless, the residual presence of S and Mo suggests that a fraction of MoS_2 flakes remained adhered to the surface, consistent with previous reports [28]. Localised areas within the groove patterns exhibited relatively higher concentrations

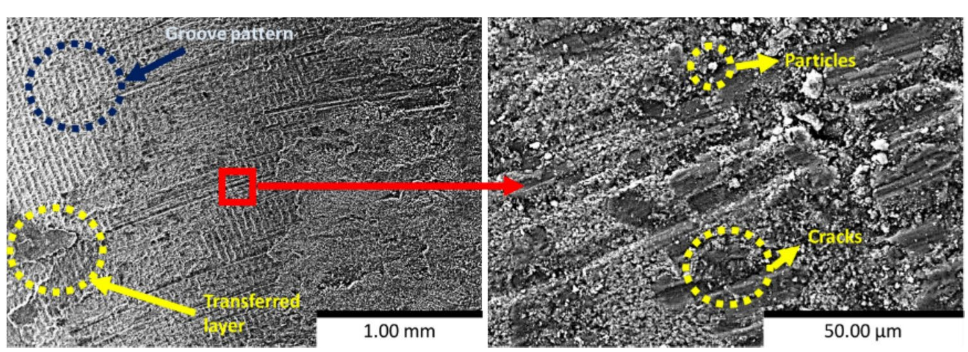

Fig. 12 SEM-SE image of a worn groove in a 75% TD MoS_2-coated texture on a 6082-T6 pin

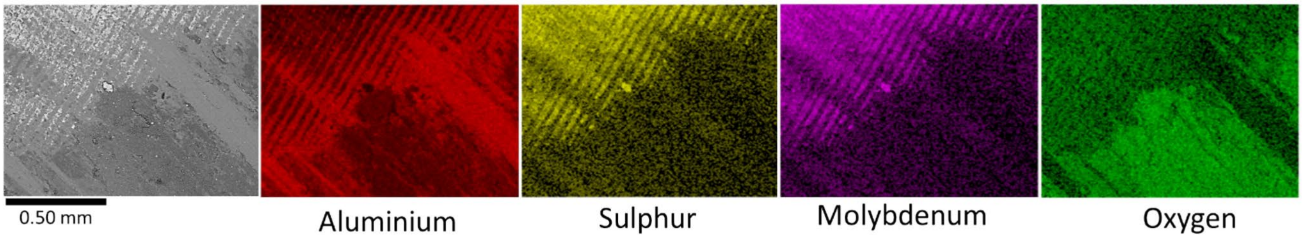

Fig. 13 EDS elemental maps of worn grooves within a MoS_2-coated groove pattern (75% TD) on a 6082-T6 pin

of S and Mo, suggesting the formation or accumulation of MoS_2 clusters during sliding.

Regions within the worn grooves also showed increased oxygen content, indicative of aluminium oxide (Al_2O_3) formation. Following MoS_2 depletion, frictional heating promoted oxidation of the exposed aluminium surface through reactions with atmospheric oxygen, leading to the formation of a thermally oxidised layer [28, 30]. Although the highest oxygen concentrations were observed in the worn grooves, oxygen was also detected in regions where the MoS_2 coating remained intact. This observation can be attributed to the formation of molybdenum trioxide (MoO_3), which likely resulted from elevated local temperatures during testing. Under such conditions, sulphur in MoS_2 can be partially substituted by oxygen, producing MoO_3 [8, 19, 28, 30]. Since MoO_3 is a relatively hard and abrasive compound, its formation contributed to scratch development and accelerated coating degradation.

5 Discussion

The present work demonstrates that laser-induced groove textures substantially improve the tribological performance of MoS_2-coated 6082-T6, with lubricant service life governed by a complex interaction between texture density, contact configuration, groove orientation, and stress distribution. By combining experimental pin-on-disc testing with finite element analysis, this study provides mechanistic insight into how surface texturing controls solid lubricant retention, release, and ultimate failure.

The surface characterization results showed that the laser-generated grooves possessed a consistent U-type geometry [39] with a depth-to-width ratio of approximately 0.1 [42], a configuration widely reported to be favorable for lubricated sliding. This geometry enabled effective storage of MoS_2 within the groove cavities while allowing gradual lubricant release during sliding. Compared with non-textured samples, all textured surfaces exhibited a pronounced extension of lubricant service life, confirming the role of grooves as lubricant reservoirs. In addition to lubricant storage, the grooves acted as sinks for wear debris, as evidenced by SEM observations of worn grooves. The ability to trap debris reduced third-body abrasion and delayed coating degradation, in agreement with previous reports on textured, solid-lubricated surfaces [12, 20, 27, 29, 30].

Texture density emerged as a key parameter controlling lubrication performance. Increasing TD consistently increased lubricant service life across all configurations, with improvements reaching up to approximately fifty times those of non-textured references. This behavior reflects the combined effects of increased lubricant reservoir volume, reduced spacing between grooves, and improved debris trapping efficiency. Higher TD reduces the extent of non-textured regions where the MoS_2 coating is thinner and more prone to early failure. Since lubricant lifespan scales with coating thickness, minimizing these weak regions delays lubricant depletion [1]. These findings highlight that texture density not only increases lubricant availability but also homogenizes the tribological surface, stabilizing the lubrication regime.

Despite the dominant influence of TD, significant differences in lubricant service life were observed between pin, disc, and pin-and-disc configurations. These differences are directly linked to the magnitude and spatial distribution of normal stresses at the contact interface, as revealed by finite element simulations. For non-textured surfaces, the disc experienced higher ejection normal stresses than the pin, explaining the shorter service life observed experimentally for the disc configuration. Since the solid lubricant ejection rate is proportional to the magnitude of the normal stress acting away from the coated surface, elevated ejection stresses accelerate MoS_2 removal [34].

Surface texturing fundamentally altered this stress landscape by introducing coexisting regions of compression and ejection stresses on the same surface. Compression stresses promoted lubricant retention within the groove cavities, while ejection stresses facilitated controlled lubricant release into the contact interface. The balance between these two stress components proved critical for sustaining lubrication, consistent with the stress-controlled lubrication framework proposed in previous studies [38]. The textured disc exhibited a larger difference between ejection and compression stresses than the textured pin, a condition shown to enhance lubrication efficiency when maintained within an optimal range [34]. In contrast, the textured pin displayed a more heterogeneous stress distribution, with highly localized stress regions that impaired the balance between lubricant retention and expulsion, leading to reduced lubrication efficiency.

The relative orientation between grooves and sliding direction further influenced lubrication behaviour, particularly for textured discs. Finite element results showed that grooves oriented at 45° to the sliding direction generated the highest ejection stresses on the disc, whereas the same orientation produced the lowest ejection stresses on the pin. Under rotational pin-on-disc testing, the 45° orientation is encountered more frequently than purely parallel or perpendicular alignments. Since ejection stress was found to play a more dominant role than compression stress in governing lubricant service life, this orientation-dependent stress amplification explains why textured discs outperformed textured pins at higher TD values. Similar behaviour was observed in the pin-and-disc configuration, where the disc retained favourable stress characteristics, while the pin showed limited sensitivity to groove orientation.

Ultimately, lubricant failure in all configurations was governed by mechanical removal of the MoS_2 coating due to sliding-induced stresses, as confirmed by friction evolution and post-test surface analysis. Once the coating was locally depleted, direct metal-to-metal contact initiated wear. SEM and EDS analyses revealed the formation of abrasive particles within worn grooves, resulting from frictional heating and oxidation processes [28, 30]. These hard oxide species acted as third-body abrasives, accelerating scratch formation and coating degradation. While thermally activated oxidation contributed to lubricant failure, it primarily acted as an accelerating mechanism rather than the root cause. After the lubricant failure, the transferred layer further began to produce as a result of the cool welding formation and its subsequent fracture. The elevated friction associated with the direct contact metal-to-metal facilitates cool welding, which is subsequently fractured by the relative motion between the bodies in contact [4, 12, 47]. The presence of the cracks following lubricant failure indicated fatigue process presence [29]. It is important to noteworthy that both the cracks formation and the cool welding generation can contribute to debris formation. Consequently, after the failure of the lubricant, the 6082-T6 underwent multiple wear mechanism, including adhesion (transferred material), abrasion (third-body), and fatigue wear (cracks).

Overall, the results demonstrate that optimal solid lubrication performance of MoS_2-coated 6082-T6 is achieved through a synergistic combination of high texture density, disc-side texturing, and favourable stress distribution. By integrating experimental observations with numerical stress analysis, this study advances the understanding of stress-mediated lubrication mechanisms and provides clear design guidelines for textured, and solid-lubricated 6XXX aluminium alloys tribological systems.

6 Conclusions

This study investigated the combined effects of laser-induced groove texture density and pin-on-disc configuration on the tribological performance of MoS_2-coated 6082-T6. Laser surface texturing produced using an infrared nanosecond-pulsed fiber laser significantly extended the solid-lubricated service life by approximately 2 to 50 times compared with non-textured surfaces, depending on texture density and contact configuration.

Increasing texture density consistently improved lubricant service life across all configurations by increasing the solid lubricant reservoir capacity, reducing non-textured regions susceptible to early failure, and enhancing debris trapping. Among the tested configurations, the pin-and-disc configuration exhibited the longest lubrication lifespan, up to 50 times greater than non-textured references, followed by the textured disc and textured pin configurations. The superior performance of the textured disc relative to the textured pin is attributed to a more favorable normal stress distribution.

Finite element analysis demonstrated that surface texturing fundamentally alters the magnitude and spatial distribution of normal stresses at the contact interface. The coexistence of compression and ejection stresses governs the balance between lubricant retention and release, with ejection stress identified as the dominant parameter controlling lubricant depletion rate. Groove orientation relative to the sliding direction significantly influenced stress distribution, with a 45° orientation producing favourable conditions for textured disc configurations and unfavourable conditions for textured pin configurations under rotational sliding.

MoS_2 coating failure was primarily driven by progressive mechanical removal under sliding-induced stresses, with possible abrasive oxide formation accelerating degradation following lubricant depletion. Overall, this work demonstrates that optimized laser-generated groove textures—particularly when applied to both contacting surfaces—provide a robust strategy for controlling stress-mediated solid lubrication and significantly extending the service life of MoS_2-coated aluminium components. Notably, multiple wear mechanisms can occur after the failure of the lubricant such as adhesion, abrasion, and fatigue wear.

Author Contributions JIAT and TTO contributed to the study's conception and design. JIAT was responsible for material preparation, data collection, analysis, and drafting the initial version of the manuscript, as well as discussion of the results. All authors reviewed and contributed to the development of subsequent versions of the manuscript. H.R.K., G.Z. and M.B. contributed to funding acquisition.

Funding The authors declare that no funds, grants, or other support were received during the preparation of this manuscript.

Data Availability No datasets were generated or analysed during the current study.

Declarations

Conflict of interest There are no conflicts of interest.

References

1. Erdemir, A.: Modern tribology handbook, 2, 787-818 (2001)
2. Hidalgo-Manrique, P., Cao, S., Shercliff, H., Hunt, R., Robson, J.: Mater. Sci. Eng., A **804**, 140751 (2021)
3. Wang, Y., Fan, F., Lin, S.: Thin-Walled Struct. **89**, 54–66 (2015)
4. Hu, T., Hu, L.: Tribol. Trans. **54**, 800–805 (2011)
5. Vazirisereshk, M.R., Martini, A., Strubbe, D.A., Baykara, M.Z.: Lubricants **7**, 57 (2019)
6. Sunil, T., Sandeep, M., Kumaraswami, R., Shravan, A.: Int. J. Mech. Eng. Technol **7**, 193–199 (2016)
7. Tang, G., Zhang, J., Liu, C., Zhang, D., Wang, Y., Tang, H., Li, C.: Ceram. Int. **40**, 11575–11580 (2014)
8. Epshteyn, Y., Risdon, T.J. In: Proceedings of the 12 Lubricating Grease Conference, pp. 28–30 (2010)
9. Arenas, M., Ahuir-Torres, J.I., García, I., Carvajal, H., De Damborenea, J.: Tribol. Int. **128**, 240–247 (2018)
10. Huang, Q., Shi, X., Xue, Y., Zhang, K., Wu, C.: Mater. Today Commun. **35**, 105854 (2023)
11. Qin, Y., Xiong, D., Li, J.: Surf. Coat. Technol. **269**, 266–272 (2015)
12. Narayana, T., Saleem, S.S.: Surf. Topogr. Metrol. Prop. **12**, 015008 (2024)
13. Ukar, E., Lamikiz, A., Martínez, S., Arrizubieta, I.: Proc. Eng. **132**, 663–670 (2015)
14. Lu, P., Wood, R.J.: Surf. Topogr. Metrol. Prop. **8**, 043001 (2020)
15. Pan, S., Jin, K., Wang, T., Zhang, Z., Zheng, L., Umehara, N.: Friction **10**, 1596–1634 (2022)
16. Karmiris-Obratański, P., Zagórski, K., Papazoglou, E., Markopoulos, A.: Int. J. Adv. Manuf. Technol. **115**, 733–747 (2021)
17. Akbarzadeh, A., Khonsari, M.: Coatings **8**, 110 (2018)
18. Mao, B., Siddaiah, A., Liao, Y., Menezes, P.L.: J. Manuf. Process. **53**, 153–173 (2020)
19. Ripoll, M.R., Simič, R., Brenner, J., Podgornik, B.: Tribol. Lett. **51**, 261–271 (2013)
20. Rapoport, L., Moshkovich, A., Perfilyev, V., Lapsker, I., Halperin, G., Itovich, Y., Etsion, I.: Surf. Coat. Technol. **202**, 3332–3340 (2008)
21. Al-Mahdy, A., Ahuir-Torres, J.I., Öpöz, T.T., Kotadia, H.R., Mullett, J., Sharp, M.C.: Opt. Laser Technol. **181**, 111626 (2025)
22. Leone, C., Genna, S.: Compos. Struct. **194**, 240–251 (2018)
23. Bunaziv, I., Akselsen, O.M., Ren, X., Nyhus, B., Eriksson, M., Gulbrandsen-Dahl, S.: Metals **11**, 1680 (2021)
24. Hummel, M., Schöler, C., Häusler, A., Gillner, A., Poprawe, R.: J. Adv. Join. Process. **1**, 100012 (2020)
25. Maharjan, N., Zhou, W., Zhou, Y., Guan, Y., Wu, N.: Surf. Coat. Technol. **366**, 311–320 (2019)
26. Kumar, V., Verma, R., Kango, S., Sharma, V.S.: Mater. Today Commun. **26**, 101736 (2021)
27. Segu, D.Z., Kim, J.-H., Choi, S.G., Jung, Y.-S., Kim, S.-S.: Surf. Coat. Technol. **232**, 504–514 (2013)
28. Voevodin, A., Zabinski, J.: Wear **261**, 1285–1292 (2006)
29. Hua, X., Xie, X., Yin, B., Zhang, P., Ji, J., Wang, H., Fu, Y.: Ind. Lubric. Tribol. **70**, 371–384 (2018)
30. Li, J., Xiong, D., Wu, H., Zhang, Y., Qin, Y.: Surf. Coat. Technol. **228**, S219–S223 (2013)
31. Uddin, M., Ibatan, T., Shankar, S.: Lubr. Sci. **29**, 153–181 (2017)
32. Zhang, H., Hua, M., Dong, G.-Z., Zhang, D.-Y., Chen, W.-J., Dong, G.-N.: Tribol. Int. **115**, 222–232 (2017)
33. Lu, L., Zhang, Z., Guan, Y., Zheng, H.: Opt. Laser Technol. **106**, 272–279 (2018)
34. Ahuir-Torres, J., Evans, S., Öpöz, T., Bashir, M., Kotadia, H.: Tribol. Int. **214**, 111303 (2025)
35. Al-Mahdy, A., Kotadia, H., Sharp, M., Opoz, T., Mullett, J., Ahuir-Torres, J.: Lasers Manuf. Mater. Process. **10**, 141–164 (2023)
36. Wu, Z., Bao, H., Xing, Y., Liu, L.: Int. J. Adv. Manuf. Technol. **114**, 1241–1277 (2021)
37. A. Internasional, (2000).
38. Xu, Z., Zhang, Q., Huang, X., Zhai, W., Yang, K., Zhu, Q.: Tribol. Int. **93**, 104–114 (2016)
39. Gropper, D., Wang, L., Harvey, T.J.: Tribol. Int. **94**, 509–529 (2016)
40. Zhan, X., Liu, Y., Yi, P., Jia, D., Xiao, P. In: Tenth International Conference on Information Optics and Photonics, pp. 154–162, SPIE (2018)
41. Ronen, A., Etsion, I., Kligerman, Y.: Tribol. Trans. **44**, 359–366 (2001)
42. Fiaschi, G., Di Lauro, M., Ballestrazzi, A., Rota, A., Biscarini, F., Valeri, S.: Tribol. Int. **149**, 105548 (2020)
43. Braun, D., Greiner, C., Schneider, J., Gumbsch, P.: Tribol. Int. **77**, 142–147 (2014)
44. Guo, L., Li, Y., Geng, S., Wang, C., Jiang, P.: Surf. Coat. Technol. **432**, 128056 (2022)
45. Zhu, Y., Fu, J., Zheng, C., Ji, Z.: Opt. Laser Technol. **83**, 21–27 (2016)
46. Xing, Y., Deng, J., Wu, Z., Cheng, H.: Appl. Surf. Sci. **265**, 823–832 (2013)
47. Hu, T., Zhang, Y., Hu, L.: Wear **278**, 77–82 (2012)
48. Saurabh, A., Verma, P.C., Dhir, A., Sikder, J., Saravanan, P., Tiwari, S.K., Das, R.: Tribol. Int. **199**, 110001 (2024)
49. Xing, Y., Deng, J., Wang, X., Meng, R.: Wear **342**, 1–12 (2015)
50. Bortoleto, E.M., Rovani, A.C., Seriacopi, V., Profito, F.J., Zachariadis, D.C., Machado, I.F., Sinatora, A., Souza, R.M.D.: Wear **301**, 19–26 (2013)